Author/s:
Brody, KM;Hampson, AJ;Cho, HJ;Johnson, P;O'Leary, SJ

Title:
A new method for three-dimensional immunofluorescence study of the cochlea

Date:
2020-07-01

Citation:
Brody, K. M., Hampson, A. J., Cho, H. J., Johnson, P. & O'Leary, S. J. (2020). A new method for three-dimensional immunofluorescence study of the cochlea. Hearing Research, 392, https://doi.org/10.1016/j.heares.2020.107956.

Persistent Link:
https://hdl.handle.net/11343/247872

Hearing Research 392 (2020) 107956

Contents lists available at ScienceDirect

Hearing Research

journal homepage: www.elsevier.com/locate/heares

A new method for three-dimensional immunofluorescence study of the cochlea

Kate M. Brody [a], Amy J. Hampson [a], Hyun-jung Cho [b], Prudence Johnson [a], Stephen J. O'Leary [a, *]

[a] Otolaryngology, Department of Surgery, University of Melbourne, Royal Victorian Eye and Ear Hospital, East Melbourne, Australia
[b] Biological Optical Microscopy Platform, University of Melbourne, Parkville, Australia

ARTICLE INFO

Article history:
Received 18 September 2019
Received in revised form
13 March 2020
Accepted 26 March 2020
Available online 5 May 2020

Keywords:
Whole cochlea imaging
Immunofluorescence
Tissue clearing
Cochlear implant
Light sheet microscopy

ABSTRACT

Visualisation of cochlear histopathology in three-dimensions has been long desired in the field of hearing research. This paper outlines a technique that has made this possible and shows a research application in the field of hearing protection after cochlear implantation. The technique utilises robust immunofluorescent labelling followed by effective tissue clearing and fast image acquisition using Light Sheet Microscopy. We can access the health of individual components by immunofluorescent detection of proteins such as myosin VIIa to look at cochlear hair cells, NaKATPase alpha 3 to look at spiral ganglion neurons, and IBA1 to look at macrophages within a single cochlea, whilst maintaining the integrity of fine membranous structures and keeping the cochlear implant in place. This allows the tissue response to cochlear implantation to be studied in detail, including the immune reaction to the implant and the impact on the structure and health of neural components such as hair cells. This technique reduces time and labour required for sectioning of cochleae and can allow visualisation of cellular detail. Use of image analysis software allows conversion of high-resolution image stacks into three-dimensional interactive data sets so volumes and numbers of surfaces can be measured. Immunofluorescent whole cochlea labelling and Light Sheet Microscopy have the capacity to be applied to many questions in hearing research of both the cochlea and vestibular system.

1. Introduction

Traditional histology and immunohistochemistry utilising serial sections and whole mount preparations has been vital for investigating cochlear histopathology. Histological dyes and antisera applied to cochlear preparations have enabled qualitative analysis of morphology and quantification of cell types present. However, tissue sectioning and whole mount preparation have some disadvantages. These techniques are both time- and labor-intensive, and qualitative and quantitative interpretation of cochlear anatomy is difficult when using 2D images – as is an appreciation of three-dimensional (3D) cochlear structure. Reconstructing the 3D cochlear anatomy from serial sections requires time consuming lateral and rotational alignment of images (MacDonald et al., 2008). Whole mount preparations of the organ of Corti with the spiral ganglion attached are a powerful technique for the detailed visualisation of hair cell survival and morphology, and ribbon and neuronal synapses, and have contributed greatly to the study of noise trauma and hidden hearing loss (Liberman et al., 2017; Sly et al., 2016). Detailed analysis of the condition of the hair cell along the whole cochlea can be gathered using this method. However, whole mount dissection destroys surrounding structures such as the spiral ligament, stria vascularis, Reissner's membrane, tectorial membrane and the spiral ganglion nerve cell bodies (Montgomery et al., 2016). Particularly relevant to the field of cochlear implantation is that any information about the tissue response to implant is lost. Another limitation is the technical difficulty and length of time for a single dissection in the guinea pig, an experimental animal commonly used in the field of cochlear implantation. In addition, due to its complex 3-dimensional shape the hook region of the cochlea is particularly difficult to dissect and reconstruct using whole mounts. This is especially the case after cochlear implantation, which causes a degree of trauma in this area. Due to the limitations of the respective techniques researchers may

*Corresponding author. Department of Surgery, Royal Victorian Eye and Ear Hospital, 32 Gisborne Street, East Melbourne, 3002, Australia. Tel.: 61 3 9929 8366.
E-mail address: sjoleary@unimelb.edu.au (S.J. O'Leary).

https://doi.org/10.1016/j.heares.2020.107956

be forced to decide between gathering detailed data about hair cells, or information about any structural or inflammatory mediated damage to the cochlea.

In the field of cochlear implant research traditional histology has enabled the study of surgical trauma, immune responses to the implant array, and potential pharmaceutical methods of protecting against post-surgical hearing loss (Braun et al., 2011; Chang et al., 2009; Connolly et al., 2011; Eastwood et al., 2010; Eshraghi et al., 2006; Farhadi et al., 2013; Kel et al., 2013; O'Leary et al., 2013; Quesnel et al., 2016; Richardson et al., 2009; Stathopoulos et al., 2014; Vivero et al., 2008). To section implanted cochleae the implant must be removed, which risks disturbing the location and integrity of the tissue response and its quantification. Furthermore, sectioning can cause structural damage to some of the finer elements of the cochlea, including the organ of Corti and the basilar, tectorial and Reissner's membranes. Visualisation of the position and morphology of Reissner's membrane is particularly important because it indicates the presence or absence of endolymphatic hydrops – a condition thought to contribute to delayed loss of residual hearing after cochlear implantation (Handzel et al., 2006; Ishiyama et al., 2016; Smeds et al., 2015). Given that Reissner's membrane can often be damaged during cochlear sectioning, traditional histology or immunohistochemistry is not ideal for accurate detection of this condition.

In contrast, whole cochlea imaging techniques such as micro-CT (Smeds et al., 2015) and Light Sheet Fluorescence Microscopy (LSFM), which have been used within our laboratory to view tissue response to implantation (Choong et al., 2019; Lo et al., 2017), do not disrupt the cochlear structure. However, imaging of the whole cochlea has introduced new challenges. Cochlear structures form complex spirals and are encased by bone which causes considerable scattering of light, even after decalcification. Both micro-CT and LSFM require chemical treatment of cochlear tissue to enable imaging. Micro-CT requires treatment with osmium tetraoxide to maximise image contrast (Wong et al., 2012), while our LSFM treatment had required harsh solvents (Spalteholz solution) to make the tissue clear enough for laser light to pass through it. LSFM and micro-CT allow visualisation of each component of the cochlea, including the exact positioning of Reissner's membrane (Buytaert et al., 2013). Recently, our laboratories have used these whole cochlea imaging techniques to determine if endolymphatic hydrops is present (Smeds et al., 2015) and visualize fibrosis (Choong et al., 2019; Lo et al., 2017) after cochlear implantation. However, these techniques are not sufficient to identify the cellular subtypes within cochlear or reparatory tissue, such as cochlear hair cells, neurons and macrophages, all of which are a measure of cochlear health and function. In 2008 MacDonald combined immunohistochemistry and clearing with Spalteholz solution in mouse cochleae (MacDonald et al., 2008). This work relied on the use of a confocal microscope, so could not be easily altered to look at larger species that are more frequently utilized in cochlear implantation research such as cats and guinea pigs. The current study outlines a technique which can be adapted to larger implanted animals (O'Leary et al., 2013) (Ryugo et al., 2005; Salt et al., 2017).

Here we present a method that although of particular interest to the study of cochlear implantation and noise trauma, could also be readily utilized to address further research interests including development of the inner ear, screening of knockout models, and characterization of genetic mutations.

2. Rationale

Researchers studying the cochlea after cochlear implantation have had to prioritise between identification of cell types present (using traditional histology and immunohistochemistry) and complete preservation cross-sectional information about the fine membranous cochlear structures (using whole cochlea imaging techniques) due to the respective strengths and weaknesses of these techniques. In cochlear implantation, there are several more issues to resolve. An analysis of the fibrotic tissue requires imaging of the scala tympani, and therefore require cochlear sectioning which can be disruptive to tissue membranous structures. However, it is also important to examine the organ of Corti, which is best achieved with whole mount imaging. Thus, analysis of both fibrosis and the organ of Corti in a single cochlea has been problematic. Furthermore, even when whole mount imaging has been chosen, it is technically challenging as the scarring associated with implantation makes dissection of the organ of Corti technically difficult. The second major consideration for cochlear implantation is that the imaging technique should ideally allow analysis of these elements while an electrode array remains *in situ*. Whilst grinding/polishing techniques where cochleae are embedded in epoxy resin can allow electrodes to remain *in situ* (Adunka et al., 2004; Wilk et al., 2016) this type of embedding precludes subsequent use of immunohistochemical labelling thus disallowing the identification of proteins *in situ* that are indicative of cellular subsets and processes. The ideal imaging method should be capable of imaging either "dummy" (silicone only) implants, or those with metallic electrode contacts which may scatter light during imaging causing a loss of signal near these electrodes.

In the current study, we aimed to develop a technique in which whole cochleae are labelled for immunofluorescence (to determine cell types that are present) and then cleared for light sheet microscopy (using non-toxic materials to minimize the associated risks to researchers) to allow us to elicit more information from each cochlea. In addition, we sought to develop a method that would allow a cochlear implant, with and without platinum contacts, to be left *in situ*. Such a technique would allow for complete and accurate visualisation of the cellular types and morphology of the tissue response to cochlear implantation, in addition to the presence and health of hair cells, neuronal projections and Reissner's membrane in the same cochlea. We also aimed to develop a technique which would allow traditional histological assessment from the same tissue after 3D imaging if required. Whilst our purposes were to develop a method for cochlear implant research we also hoped to discover a method which can be readily applied to hearing research and a wide variety of questions regarding cochlear and vestibular function.

3. Description of the methods

3.1. Experimental design

All experimental procedures were completed in accordance with the Royal Victorian Eye and Ear Hospital's Animal Research Ethics Committee (ethics approvals 18/395AU, 18/361AU). Adult pigmented Dunkin-Hartley guinea pigs were unilaterally implanted with a silastic dummy cochlear implant and then allowed to recover. Left cochleae were implanted, while right cochleae served as unimplanted controls. Two weeks after cochlear implantation, guinea pigs were euthanised and their cochleae collected. Cochleae were then prepared for 3D immunofluorescence and imaging. Dummy cochlear implants were left *in situ* to confirm that the technique could be carried out with the dummy implant still in place.

In addition, one guinea pig's left cochlea was implanted with a stimulating cochlear implant. This guinea pig was euthanised six weeks after implant surgery, having received five hours of electrical stimulation per day via the implant for a period of four weeks. The cochleae were then collected; the right cochlea served as an

unimplanted control. This guinea pig was included to confirm that the technique could be carried out on an electrode array with platinum contacts.

3.2. Implanted arrays

The bulk of this study was carried out using a silicone only dummy electrode 0.4 mm in diameter and typically inserted to a depth of ~2.5 mm. The stimulating array comprised eight platinum bands and had a width diameter of 0.3 mm at the tip and 0.425 mm at the base, and height diameter of 0.2 and 0.275 mm at the tip and base respectively. It was inserted to a depth of ~5 mm.

3.3. Implant surgery

Guinea pigs were anaesthetised using intramuscular ketamine (60 mg/kg, Troy Laboratories, Sydney, Australia) and xylazine (4 mg/kg, Troy Laboratories, Sydney, Australia), and local analgesia was provided at the incision cite using lignocaine (1 mg/ml, Troy Laboratories, Sydney, Australia). A post auricular incision was made, and the muscle overlying the bulla retracted. A superior bullostomy was performed with a 1.8 mm cutting bur to expose the basal turn of the cochlea, followed by a cochleostomy made with a 0.6 mm diamond bur. The cochleostomy was positioned approximately one mm from the round window niche. The array was then slowly and carefully inserted until resistance was felt. The cochleostomy was sealed around the array with a muscle plug. Dummy arrays were trimmed at the level of the bullostomy. The stimulating array was anchored to the skull using tissue adhesive and Dacron mesh, and then passed under the skin to a small exit wound near the scapulae to allow daily stimulation via connection to a speech processor (Nucleus Sound Processor, Cochlear Ltd). The post auricular wound was then sutured in two layers. All animals were then given a subcutaneous injection of analgesia (0.03 mg/kg; Temgesic, Reckitt Benckiser, Australia) and allowed to recover prior to returning to their pre-operative housing for the length of the experiment.

3.4. Cochleae harvesting and preparation

Two weeks after implantation (for dummy implants) or six weeks after implantation (for the simulating array), guinea pigs were euthanised with an intraperitoneal injection of 2.5 ml of pentobarbitone (325 mg/ml; Virbac, Sydney, Australia). Guinea pigs were then transcardially perfused with 0.9% normal saline followed by 10% neutral buffered formalin, and cochleae were harvested. Once removed, cochleae were placed in 10% neutral buffered formalin overnight at room temperature and rinsed with phosphate buffered saline (PBS) before decalcification in 10% (w/v) ethylenediaminetetra-acetic acid (EDTA) at room temperature for 2.5 weeks with 20 ml changes every two days. Decalcified cochleae were trimmed of excess bone, and a small perforation was made at the apical tip to allow antibodies to diffuse through the cochleae. Permeabilisation was performed by three 10-min changes in dimethyl sulphoxide (DMSO) followed by three 20-min changes in PBS with agitation. Cochleae were further permeabilised by pre-incubation in PBS with 1% Triton (PBS-T) and 5% Normal Goat Serum for at least 2 h. This step could be extended to overnight agitating at 37 °C without compromising on quality. Cochleae were then incubated in primary antibodies for three days agitating at 37 °C (see Table 1 for concentrations). Both the left implanted and right control cochleae were incubated in the same 2 ml vial of antibody to decrease labelling variability and save antibody. After primary antibody incubation, cochleae were washed in PBS-T (20 ml) at least three times while agitating at 37 °C and were then incubated in secondary antibodies overnight (see Table 2), agitating at 37 °C. The cochlear washing in PBS-T (20 ml; at least 3 times), during agitation at 37 °C was then repeated. The temperature was altered to 4 °C and tissue was washed twice in PBS (20 ml) to remove the Triton X. The cochleae were then placed in serial dilutions of ethanol with pH > 9.0 (50%, 70%, 100%, 100%) for up to 12 hours each, agitating at 4 °C. Finally, cochleae were removed from ethanol and submerged in ethyl cinnamate overnight at room temperature.

To image whole cochleae, Ultramicroscope II (LaVision BioTec, Bielefeld, Germany) with an Olympus MVPLAPO 2x lens (NA: 0.5) attached to a stereomicroscope (MVX10 with Zoom body 0.63x – 6.3x) was used to achieve a final magnification range from 1.26x to 12.6x. The lightsheet was generated by diode laser (488, 561, 639 nm wavelengths) and the emitted signal was filtered with a specific filter (as specified in Table 3) before being detected with sCMOS camera (Andor Neo 5.5, pixel size 6.5 μm x 6.5 μm, 2560 × 2160 pixels) at 250 ms exposure. Images were acquired using ImspectorPro software (version 5.1.328, LaVision BioTec, Bielefeld, Germany) in 16-bit tiff image format. The pixel size of image was dependent on the final zoom of the microscope, such that it was 4.797 μm at 1.26x and 0.480 μm at 12.6x. The Z-step size was set to 5 or 10 μm for all measurements yielding 250–500 images per sample and the acquisition took generally 2–3 minutes per laser wavelength.

3.5. 3D image analysis

Raw tiff images generated from Ultramicroscope II were converted as Imaris file (.ims) using Imaris™ file converter (v9.2.1, Oxford Instruments, Abingdon, UK) and visualised in 3D with Imaris™ software (v9.2.1, Oxford Instruments, Abingdon, UK). To generate a frequency map on the 3D image, whole cochleae were imaged at magnification 1.26x where the line of hair cells was clearly visible. Hair cells were traced as a 3D 'filament' object using a 'Filament tracer' module (Fig. 1A). Each voxel point of the filament corresponding to the frequency position was placed with a new spot object using 'Filament Analysis' XTension, a MATLAB plugin available for Imaris™ XT module (Fig. 1B). The x, y, z position of each point was exported and its accumulative distance from base was calculated in three dimensions. The frequency map was calculated using Equation (1) published in (Tsuji et al., 1997):

$$\%d = 66.4 - 38.2 \log(kHz) \quad (1)$$

where *%d* corresponds to percent distance from base of the cochlea and *kHz* represents a characteristic frequency. The representative frequency positions are annotated in Fig. 1C. Selected areas along the organ of Corti were then imaged at higher magnification and 3D surfaces of inner and outer hair cells were rendered for volumetric measurement. 3D surface reconstruction was performed using automatic creation wizard for objective and reproducible detection. Within the wizard, signal smoothing was omitted in order to preserve detailed structure and the segmentation threshold was determined automatically using an algorithm based on (Ridler et al., 1978) followed by background subtraction to enhance local contrast. Each reconstruction setting was saved to apply in future studies. Likewise, 3D surfaces of the myo-fibrotic and giant cells were rendered for volumetric measurement, and individual macrophages were reconstructed as 3D spots with an average diameter (15 μm) for automated cell counting.

3.6. Resin processing

After 3D immunofluorescence was completed, several cochleae underwent an altered Spurr's resin processing protocol to test the

Table 1
Primary antibodies.

Epitope	Host Raised	Company	Concentration	Catalogue
Myosin VIIa	Rabbit	Proteus	1:400	25–6790
Neurofilament Heavy chain	Chicken	Milipore	1:1000	AB5539
NaKATPase alpha 3	Mouse IgG1	Invitrogen	1:400	MA3-915
IBA1	Rabbit	Wako	1:400	019–19741
Smooth Muscle Actin	Mouse IgG2a	Sigma	1:400	A2547
Tyrosine Hydroxylase	Chicken	Milipore	1:400	AB9702

Table 2
Secondary antibodies.

Life Technologies Secondary Antibodies	Concentration	Catalogue
Goat anti-Rabbit IgG (H + L) Alexa Fluor Plus 647	1:500	A-21125
Goat anti-Chicken IgY (H + L), Alexa Fluor 594	1:500	A-11042
Goat anti Rabbit IgG (H + L) Alexa Fluor 488	1:500	A-11078
Goat anti Mouse Alexa Fluor IgG2a 647	1:500	A-21241
Goat anti Mouse Alexa Fluor IgG1 594	1:500	A-21125

Table 3
Laser details.

Laser	Output	Emission Filter
488 nm	85 mW	525/50
561 nm	100 mW	620/60
639 nm	70 mW	680/30

validity of performing traditional histology after the presented technique.

Cleared cochleae immersed in ethyl cinnamate were transferred to three changes of acetone under vacuum. The solution was replaced with 1:1 ratio of acetone to Spurr's resin placed under vacuum for two hours. The 1:1 solution was then removed and replaced with a 3:1 ratio of Spurr's resin to acetone solution for 12 hours. The 3:1 Spurr's/acetone solution was removed and replaced with 100% Spurr's resin solution for five hours, followed by one more change into 100% Spurr's resin overnight. The specimen was embedded in a mould using fresh Spurr's resin and cured overnight in a 65–70 °C oven. The specimen was removed from the mould, orientated, and cut at 2 μm using a Leica microtome with a ralph glass knife. The cut sections were then incubated at 70 °C for 2 h before de-spurring (using saturated sodium hydroxide in ethanol) and stained with Gills V Haematoxylin and aqueous Eosin.

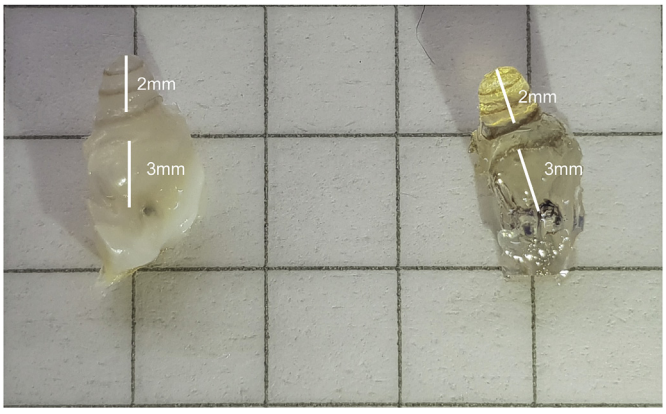

Fig. 2. Comparison of an uncleared, decalcified cochlea and one that has been cleared with ethyl cinnamate. There is no significant shrinkage of the tissue, thus volumes can be measured accurately. Scale grid: 6 mm.

4. Results

Guinea pig cochleae that have been immunofluorescently labelled then dehydrated and cleared do not show any major size or shape alterations even though the appearance is now completely transparent (Fig. 2). Therefore, in contrast with other clearing techniques (Buytaert et al., 2014) (Hama et al., 2015) (Azaripour et al., 2016), measurements made from imaging of cochleae will be accurate and no major shrinkage or expansion adjustments are necessary to maintain data integrity. This result mirrors another study which also found an ethyl cinnamate clearing technique was the most resistant to shrinkage (Klingberg et al., 2017). A complete assessment of all of the internal elements of the cochlea such as the length of the organ of Corti and size of spiral ganglia are yet to be made and some shrinkage cannot be completely ruled out.

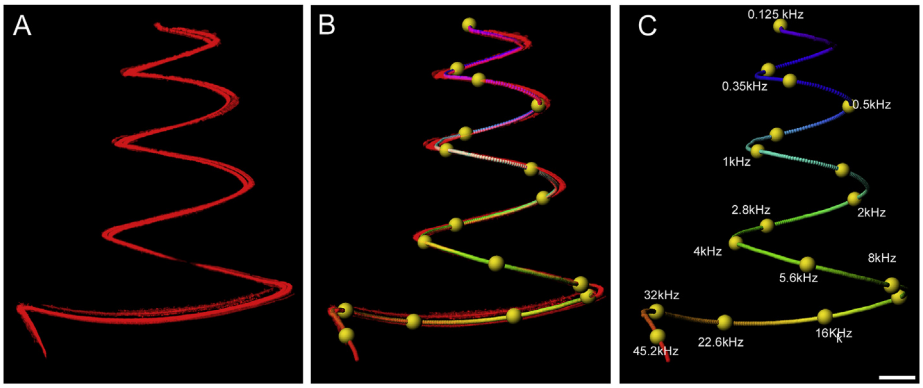

Fig. 1. A) Labelling with antisera to Myosin VIIa within hair cells in the organ of Corti. **B)** Measurement of the length of the organ of Corti using Imaris and Matlab to calculate the frequencies corresponding to each area of the cochlea. **C)** Representative frequency positions, as calculated using Equation (1) (Tsuji et al., 1997). Scale bar for A–C: 300 μm.

UltraMicroscope II utilises three thin light sheets: one horizontal and two angled at around 11° from horizontal, merging at the centre to illuminate the sample homogenously and to minimize stripe artefacts. We trialed mounting cochleae in many different orientations to minimize distortion of the signal by bone attached at the basal end. The most effective orientation was to have the cochleae mounted in a specific direction where the apical side of cochlea is located at the illumination side (Fig. 3). All cochleae included in this study were mounted in this way. Emitted fluorescence light is detected with a sCMOS equipped microscope that is mounted perpendicular to the plane illumination. By moving the sample through the light sheets a 3D image stack at cellular resolution can be generated (Dobosz et al., 2014). A combination of this technology, intense immunofluorescent labelling, and very effective clearing of tissue inclusive of the bone, allows complete visualisation of multiple components of the cochlea. Bleaching of the sample was not observed with the lasers used as laser power could be maintained at a low level and exposure time maintained at 250 ms.

Implanted cochleae within the study were imaged with the implant still *in situ*, however it must be noted that the implant itself is not fluorescently labelled and therefore will not be visible in the three dimensions. This means that the cellular components of the tissue response to implantation (which encapsulates the cochlear implant) remains intact; a unique characteristic of the presented methodology. Previously the removal of the implant as well as sectioning or dissecting has disrupted the tissue response.

4.1. Assessing cochlear structures

Fig. 4 indicates an unimplanted cochlea (A-D), an implanted cochlea (E-H) and a high magnification image of the implanted cochlea (I-L), while Fig. 5 indicates an unimplanted cochlea (A-D), an implanted cochlea (E-H) and a high magnification of an implanted cochlea showing a maximum intensity projection of 10 slice images 5 μm apart (I-L).

In Fig. 4A, E and I we demonstrate labelling with Myosin VIIa – a motor protein essential to the functioning of stereocilia within hair cells – enabling gross information about the organ of Corti to be assessed. While the resolution with this technique is not as high as that achieved with whole mount techniques, the ability to undertake complete analysis of the intact organ of Corti – without the tissue disruption associated with difficult surface preparation dissections or the alignment and sampling challenges intrinsic to serially sectioned histology slides – provides an opportunity to study both the organ of Corti and pathological changes within the cochleae walls and scala in the same specimen. This is of interest whenever exploring the pathology of hearing loss associated with cochlear stress (such as cochlear implantation, noise exposure, ototoxicity, and infection), where the loss of sensory or neural cells may be related to the broader cochlear response to injury, and involve inflammation, necrosis or endolymphatic hydrops. Fig. 4B, F and J, and Fig. 5C, G and K also showcase neuronal labelling in the form of NaKATPase α3, providing an opportunity to study long term trauma and neuronal changes in the cochlea. In addition, Fig. 5B, F and J demonstrates labelling with tyrosine hydroxylase (TH) which is present in neuronal fibres originating from the noradrenergic sympathetic neurons and a subset of dopaminergic efferent neurons projecting from the lateral olivocochlear region. The ability to view this neuronal signal in three dimensions raises the possibility of studying long term interventions to assess neuroplastic changes to the extrinsic neuronal connections within the inner ear. To further verify the integrity of our immunofluorescence, Supplementary Fig. 1 shows a control in which the primary antibodies are omitted. The lack of visible selective labelling indicates the antisera used are indeed specific for the proteins of interest.

In addition to visualising the organ of Corti, this whole cochlea imaging technique allowed visualisation of delicate cochlear structures such as Reissner's membrane, the assessment of which is required to quantify endolymphatic hydrops; a pathological response of the cochlea to various forms of stress, including cochlear implantation, noise exposure or Meniere's disease. Endolymphatic hydrops may be associated with any cochlear inflammation and is known to cause secondary sensorineural hearing loss through degeneration of cochlear hair cells and synaptopathy. When endolymphatic hydrops is present, its extent is quantified by bowing and lengthening of the membrane, and this is best visualised with whole cochlea methods, as demonstrated previously by Smeds and colleagues from micro-CT analysis of the cochlea (Smeds et al., 2015). Interpretation of endolymphatic hydrops with cochlear sectioning techniques is fraught because Reissner's membrane is very delicate and can be distorted or torn during processing or sectioning. An assessment of endolymphatic hydrops is not possible with surface preparation techniques, because Riessner's membrane is removed

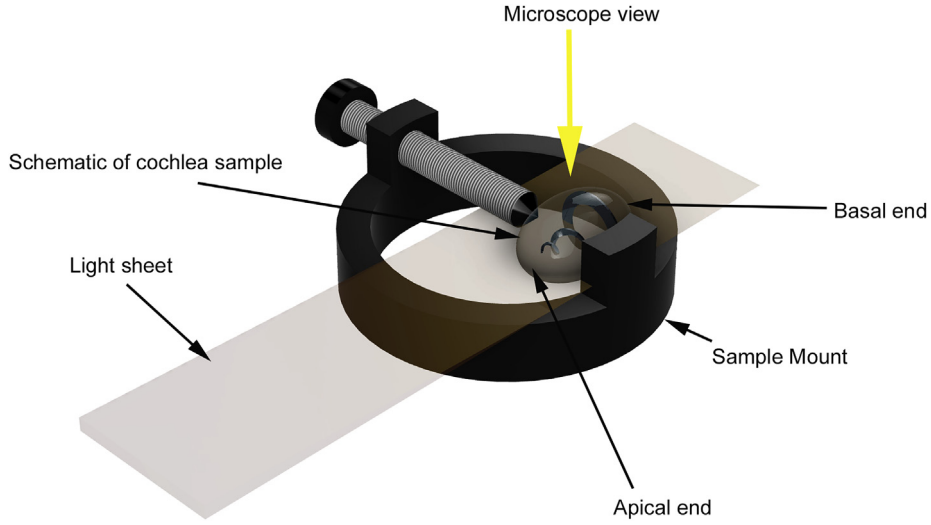

Fig. 3. A schematic showing the optimal sample mounting to view and gather data. A screw holds the tissue in place. The light sheet from the apical end of the of the cochlea sample is used to illuminate the sample; this is to decrease the light diffraction by the bone at the basal end of the cochlea. The detection objective is positioned above the sample.

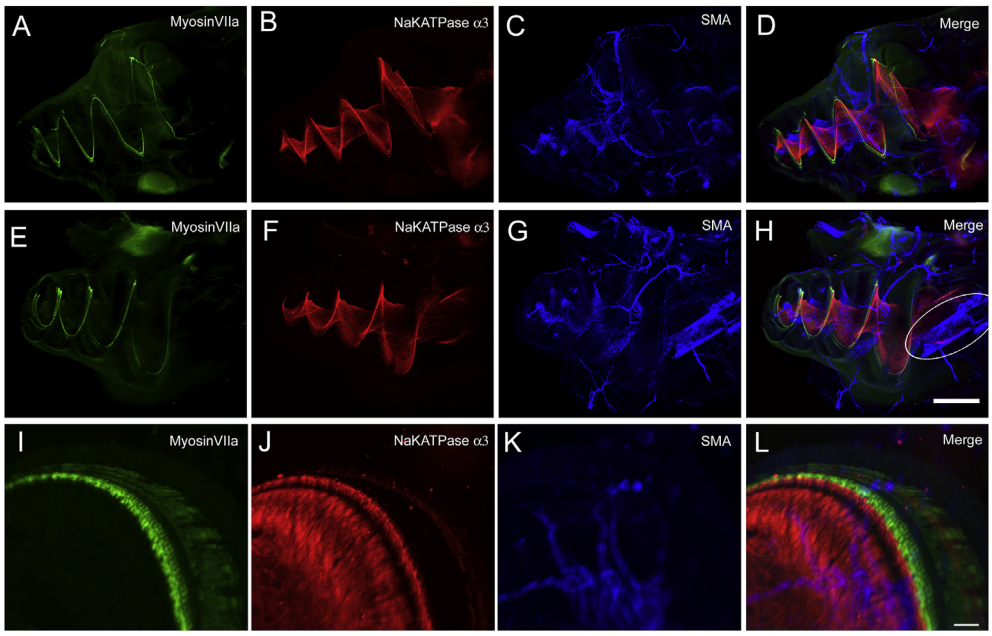

Fig. 4. A-D) Triple labelling of an unimplanted cochlea, and **E-H)** a cochlea implanted with a silicon electrode. This figure displays binding of antisera raised against Myosin VIIa, labelling both inner and outer hair cells within in the organ of Corti (A&E); binding of antisera raised against NaKATPase alpha 3, labelling the afferent neurons within the spiral ganglia and neural projections (B&F); and binding of antisera raised against smooth muscle actin (SMA), labelling both the arterioles within the cochlea (C&G) and fibroblasts that transiently express this protein during the wound healing process (G). At two weeks post-implantation, SMA is observed to surround the electrode (G). Merged images are displayed (D&H), with the myo-fibrotic tissue response marked by the oval. Scale bar for A–H: 600 μm. **I-L)** High magnification (12x) of hair cell and neuronal contacts showing morphological detail in the middle turn of the implanted cochlea. Scale bar for I–L: 30 μm.

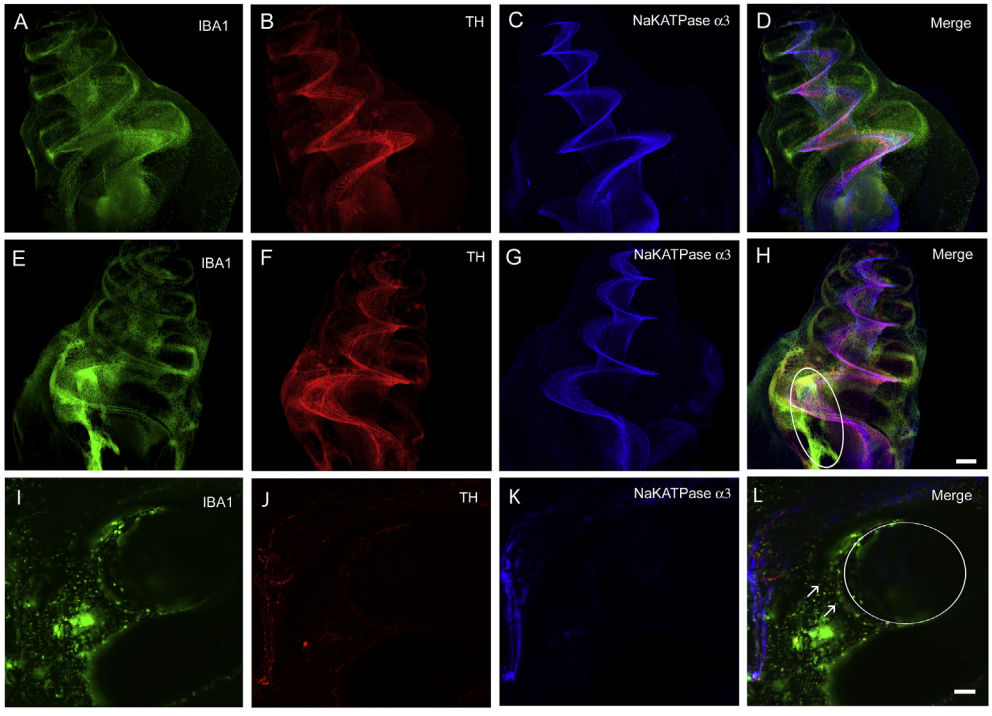

Fig. 5. A-D) Triple labelling of an unimplanted cochlea, and **E-H)** a cochlea implanted with a silicon electrode. This figure displays binding of IBA1 antisera, labelling resident macrophages in the cochlea (A&E); binding of antisera to Tyrosine Hydroxylase (TH), labelling the sympathetic neuronal fibres, dopaminergic efferent neuronal fibres within the spiral ganglia, and neural projections (B&F); and binding of antisera to NaKATPase alpha 3, labelling the afferent neurons within the spiral ganglia and neuron projections (C&G). At two weeks post-implantation, the IBA1 labelled cellular inflammatory reaction to the silicon dummy electrode shows that activated macrophages form giant cells and surround the electrode (E). Merged images are displayed (D&H), with the inflammatory tissue reaction to the silicon electrode marked by open oval. Scale bar for A–H: 300 μm. **I-L)** Shows a maximum projection of 10 slice images 5 μm apart in an implanted cochlea to indicate the capacity for cellular detail to be obtained. The electrode is again indicated by oval and macrophages are indicated by arrows (L). Single extrinsic fibres labelled with antisera raised against TH are clearly visible in panel J. Scale bar for I–L: 30 μm.

and the visualisation is orthogonal to the membrane. The light sheet methodology described here allows an assessment of both endolymphatic hydrops, the organ of Corti, and other markers of inflammation within the cochlear walls. Supplementary Fig. 2 shows a single slice captured during the image acquisition of an IBA1 labelled control non-hydropic cochlea. Note that Reissner's membrane is straight, as expected when there is no morphological evidence for endolymphatic hydrops.

4.2. Assessing inflammation and fibrosis

The composition of the cellular components of the tissue response to the cochlear implant have been historically studied using serial sections with histology and immunohistochemistry. The current technique allows 3D reconstruction of the tissue reaction without the labour and time necessary for both for sectioning and stereological analysis of the volume and cell numbers in the tissue reaction. In Fig. 4C, G and K, the control (unimplanted) and implanted cochleae were co-labelled with smooth muscle actin (SMA), which is not only present in arterioles within the cochlea but is transiently expressed by fibroblasts in the wound healing process. Fig. 4G and H demonstrate a dense layer of fibroblasts surrounding a silicon implant (outlined in Fig. 4H). See also Supplementary Figs. 3 and 4 for video representation of light sheet microscopy and 3D reconstruction and rotation of the image constructed in Imaris. Fig. 5A, E & I show labelling with antisera to IBA1 protein present in quiescent and upregulated in activated macrophages. The increased number of and activation of macrophages in response to the addition of a silicone implant for 2 weeks is visible in Fig. 5E (and outlined in Fig. 5H). Fig. 5I-L shows a maximum intensity projection of 10 slice images 5 μm apart to indicate the capacity for cellular detail to be obtained; in Figure 5L the position of the electrode is outlined, and macrophages are indicated by arrows. Single extrinsic fibres labelled with antisera raised against tyrosine hydroxylase are clearly visible in Fig. 5J. All the antisera tested for this 3D immunofluorescent labelling technique were validated in at least three different cochleae.

Supplementary video related to this article can be found at https://doi.org/10.1016/j.heares.2020.107956.

We have shown that imaging an implanted cochlea with a stimulating array *in situ* is indeed possible. Fig. 6 shows a cochlea implanted with a stimulating array labelled with both SMA and neurofilament heavy chain. The metal electrodes do not interfere with the laser in any of the fluorescent channels, and the tissue reaction to the electrode can still be visualised and its individual components quantified. The tissue response to the electrode is highlighted with the oval in Fig. 6C. This tool will be invaluable in the study of hearing protection after cochlear implantation.

4.3. Potential for 3D quantification

As described in Section 3.5 we have used the Imaris filament tool to trace and measure the length of the organ of Corti, then retrieved 3D positions of hair cells to partition the organ into a frequency map (Fig. 1). Creation of this frequency map allowed detailed analyses of hair cells at frequency-specific locations. In Fig. 7A apical and basal areas of the cochlea were selected corresponding to frequencies of 0.25 and 32 kHz respectively and analysed in detail. High magnification images were taken at 12.6x (Fig. 7B and D). Hair cell labelling was then rendered as a 3D surface and the surfaces were categorised as inner and outer layers based on their x,y,z location, with automatic threshold and background subtraction to avoid biased detection (Fig. 7C and E). The total volume of each layer can be measured within specified regions of interest. Although this method does not provide the specific number of hair cells present, the volume of the layer of hair cells can be compared between cochleae to provide a degree of quantification. This type of analysis can measure a volume change but will not specify a cause, an example of which could be hair cell loss or shrinkage – a common response to the trauma of cochlear implantation (Jia et al., 2013). The combination of low magnification construction of the frequency map and the high magnification imaging for assessing any alteration in the volume of the hair cells layers provides a useful tool in the study of health of the organ of Corti and gross neuronal changes after cochlear implantation, noise or other trauma.

In addition, Imaris™ software was used to measure the volume of the myo-fibrotic response, count the number of macrophages and define surfaces of giant cells. Images at higher zoom (2.5x – 12.63x) were imported and subjected to surface reconstruction as described in Section 3.5. Fig. 8A shows the fibrotic reaction around the implant, exhibiting cells expressing SMA which is believed to be expressed transiently during healing; this labelling can then be rendered as a surface which corresponds to the volume of the reaction (Fig. 8B). The size of the tissue response, mean intensity of labelling, and other parameters could be calculated to

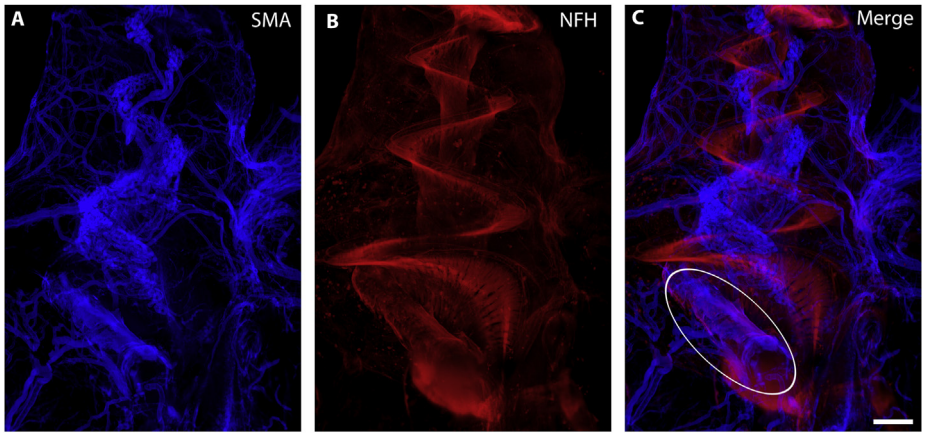

Fig. 6. A cochlea implanted with a stimulating electrode for 6 weeks. The electrode array was left *in situ* during both processing and imaging. **A)** Binding of antisera raised against smooth muscle actin (SMA), labelling both the arterioles within the cochlea and fibroblasts expressed during wound healing. **B)** Binding of antisera raised against neurofilament heavy chain (NFH), labelling afferent neurons within the spiral ganglia and neural projections. **C)** Merged image, with oval showing the position of the implant. The metal electrodes do not interfere with image capture in any of the fluorescent channels. Scale bar: 300 μm.

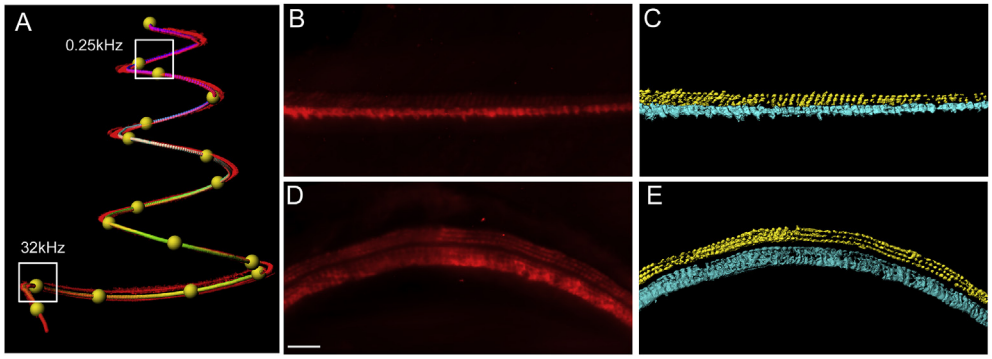

Fig. 7. A) Measurement of the length of the organ of Corti using Imaris and Matlab to calculate the frequencies corresponding to each area of the cochlea boxes indicate area sampled. **B&C)** Apical hair cells at a frequency of 0.25 kHz corresponding to box imaged at 12.6x magnification. Then rendered as a surface to allow quantitative analysis of loss or shrinkage of the hair cells. **D&E)** Basal hair cells imaged at a frequency of 32 kHz corresponding to box imaged the rendered as a surface to allow quantitative analysis. Scale bar for D–G: 100 μm.

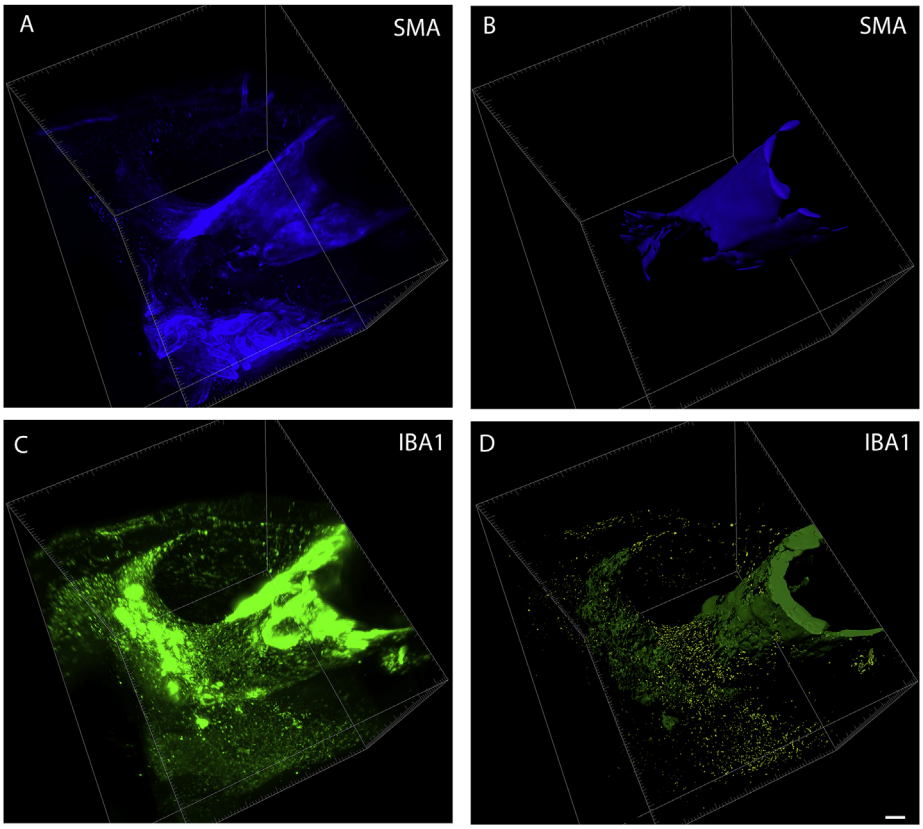

Fig. 8. A) Smooth muscle actin labelling in the myo-fibrotic tissue response. **B)** Volume render of smooth muscle actin labelling, allowing quantification of the fibrotic reaction. **C)** IBA1 labelling of macrophages. **D)** Volume rendering of the macrophages (light green) and multinucleated giant cells (dark green). Using a cell counting algorithm the number of macrophages can be counted. Scale bar: 100 μm.

quantitatively analyse the tissue response. Fig. 8C shows single macrophages and giant cells surrounding the myo-fibrotic response to the silicon implant, while Fig. 8D displays the subsequent volume rendering of the macrophages. To analyse the inflammatory response, information about macrophage size and shape is entered into a surface detector tool. The cells that fit the characteristics of a macrophage (using the aforementioned properties) can then be counted; separate macrophages are shown in light green. Multinucleated giant cells, which are detected as a separate object given they don't fit the set characteristics of a macrophage, are shown in dark green.

Finally, we have shown that the cochleae may still be sectioned after clearing and imaging by embedding in Spurr's resin if further morphological detail is required from the cochlea post imaging for light sheet microscopy. This may be of interest in the context of long-term studies and large animal research to be aware that immunofluorescent labelling and clarification of cochleae does not rule out conventional histological study and quantification techniques. Fig. 9 shows fine resin sections stained with H&E showing excellent maintenance of morphological integrity.

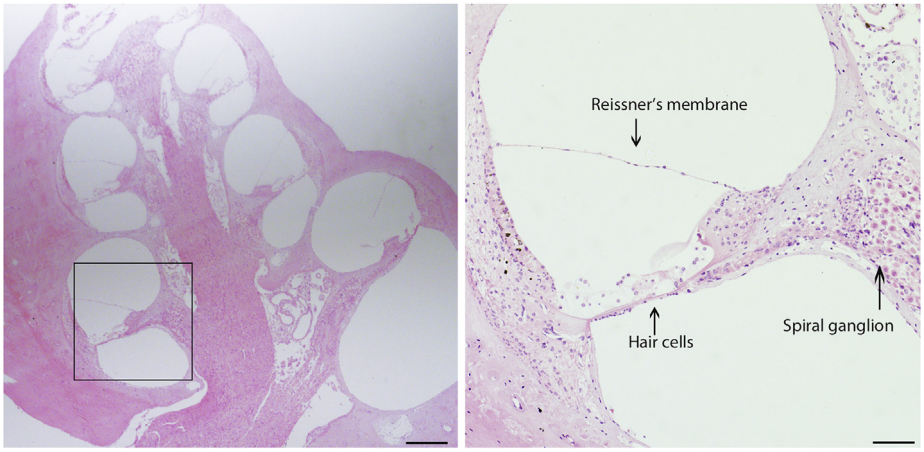

Fig. 9. Photomicrographs of an unimplanted cochlea that has been processed for immunofluorescence and subsequent clearing, and has then undergone alternate processing for Spurr's resin sectioning and haematoxylin and eosin staining. Both low and high magnification images indicate conventional histological (H&E) staining, showing well maintained tissue structure. This indicates our technique is indeed compatible with traditional histological techniques, which can be performed after imaging on the Ultramicroscope II. Scale bar: 400 μm (left panel) and 100 μm (right panel).

5. Discussion

The whole cochlea immunofluorescence followed by tissue clearing technique outlined here is a powerful tool to access detailed 3D data on tissue and cellular markers in addition to different aspects of cochlear structure. Combining the technique with image processing packages such as Imaris™ provides functionality for the visualisation, segmentation and interpretation of 3D and 4D microscopy datasets, using tools to segment large datasets to identify, separate, and visualize individual objects. Many studies have validated the data obtained via 3D imaging in comparison to conventional histological 2D analysis, showing increased accuracy in quantification resulting in sensitivity to differences (Basu et al., 2018) (Puelles et al., 2016). The 3D immunofluorescence labelling technique described here combined with the use of image processing packages allows enumeration and analysis of the volume and shape of macrophages in response to implantation or other foreign bodies.

The light sheet microscopy system used in the current study has some advantages that it provides, including a large field of view and fast acquisition optimal for the whole tissue imaging. However, future implementation of this technique on single cell counting should be done with additional consideration. At the highest magnification (12.6x) the lateral resolution is sufficient to distinguish cellular borders of spiral ganglion neurons and the dark patches of nuclei enable cell counting analyses (although not shown here). In contrast, the borders of hair cells labelled with Myosin VIIa cannot be readily defined, especially if the cell is oriented axially meaning that individual hair cell counting may be inaccurate. One of the main factors limiting the axial resolution of this system is the thickness of the light sheet, which is around 5 μm. Reducing the light sheet thickness would enhance the axial resolution but this would narrow down the area able to be imaged due to the shortened waist of Gaussian beam and this will increase the acquisition time significantly longer and requires additional image computation. If sub-cellular levels of resolution are required, researchers may consider alternative approaches such as using light sheet microscopy equipment which generates thinner light sheets. However most currently available techniques have limitations either in imaging dimension, acquisition time, computation requirements or light efficiency (Power et al., 2017). Thus, other tissue preparation and imaging techniques must then be considered such as sectioning or whole mount preparation and light or confocal microscopy so that the distance from the sample is then reduced to allow for increased resolution. The tradeoff is between the size of the sample and resolution possible. Furthermore, the degree of quantification of the organ of Corti needs to be traded off against other information gleaned on cochlear pathology from whole cochlea imaging.

That said, our 3D technique does provide data about the health of hair cells and neuronal tissue and allows gross quantification of hair cells across a specific cochlear region using volumetric analyses, which can be compared across treatment groups (Fig. 7). Analyses of volumes rendered can be useful in cochlear implant research – the acute or chronic trauma the cochlea is exposed to, with associated cochlear fibrosis, may make the preparation of whole mounts technically difficult and the dissection itself will often result in damage to the organ of Corti. This is particularly pertinent to the basal turn(s) of the cochlea where an implant may be found. In the field of cochlear implant research, the data from volumetric analyses – though potentially not as finely granulated – would be more intact, quantifiable and reproducible and thus would be more reliable than whole mount preparation. This type of analysis would not only encapsulate whether there is a loss in the number of hair cells but also shrinkage of hair cells; a common response to cochlear trauma (Jia et al., 2013). This, together with the advantage that a cochlear implant can be left *in situ* so that histopathological changes can be directly related to the position of the implant will have many benefits. Within the field of noise induced hearing loss our technique would pick up physiologically meaningful hair cell losses such as notches in response to noise trauma.

An additional limitation is the number of antibody markers that can be used at a time per cochlea. Using the Ultramicroscope II, we had five lasers available to us, and therefore only five immunofluorescent markers could be viewed per cochlea. Viewing combinations of markers can be also limited by the species in which the primary antibodies are raised. Serial sections and stereological methods are thus still required if a large number of cellular markers (for example antibodies against specific inflammatory cell subtypes) are required to be viewed per cochlea.

Whole cochlea immunofluorescence and light sheet microscopy provides a powerful tool to examine the cochlea after cochlear implantation, particularly in terms of determining how surgical approach or electrode design and position can alter the foreign

body tissue response. All whilst improving efficiency by decreasing the time, labour and animal numbers needed to address research questions. However, immunofluorescence viewed in three dimensions allows structural, tissue type and cellular information to be gathered in parallel, and this holds strong potential to answer broader research questions about the cochlear response to injury. For example, the ability to look at the innervation of the cochlea unobstructed by other tissue types, to be able to rotate and measure different structural elements, and then to compare the structure and protein expression at (for instance) different developmental milestones could result in great insight into neurodevelopment. In addition, our 3D technique would provide an excellent screening tool to assess the structure of the cochlea and vestibular system (and other tissues) in knockout mouse models and while characterizing genetic mutations; this technique can be adapted readily to mouse tissue (unpublished observations). Finally, the technique may be of use while examining the response of the inner ear to various potential therapeutic approaches, such as using hydrogels to deliver pharmaceutical agents (Wise et al., 2016) or using stem cells or viral vectors to deliver genetic therapies (Richardson et al., 2015) (Ito et al., 2001).

6. Conclusions

Our technique allows a remarkable degree of qualitative and quantitative data to be produced from one cochlea, including the health of hair cells and neuronal tissue, differentiation between afferent and efferent neurons, and different stages of the inflammatory process, all of which are relevant to any study of cochlear stress, injury or surgery. It utilises robust immunofluorescent labelling with markers for proteins of interest followed by dehydration and clearing with non-toxic ethyl cinnamate, then utilization of cutting-edge technology for large scale fluorescent imaging.

CRediT authorship contribution statement

Kate M. Brody: Conceptualization, Investigation, Methodology, Validation, Data curation, Writing - original draft. **Amy J. Hampson:** Investigation, Methodology, Project administration, Writing - original draft. **Hyun-jung Cho:** Methodology, Software, Data curation, Writing - review & editing. **Prudence Johnson:** Investigation, Methodology, Writing - review & editing. **Stephen J. O'Leary:** Conceptualization, Writing - review & editing, Funding acquisition.

Acknowledgements

The authors would like to thank Samantha Moreland for animal husbandry assistance, Helen Feng for electrode manufacture, Dr Gabriela Segal from the Biological Optical Microscopy Platform, University of Melbourne for imaging assistance, and Dr Aaron Collins for assistance in preparing figures. This work was funded by the National Health and Medical Research Council (Australia; GNT1125970), the Garnett Passe and Rodney Williams Memorial Foundation, and a generous bequest from the family of the late Gordon Darling, AC.

Appendix A. Supplementary data

Supplementary data to this article can be found online at https://doi.org/10.1016/j.heares.2020.107956.

References

Adunka, O., Unkelbach, M.H., MacK, M., Hambek, M., Gstoettner, W., Kiefer, J., 2004. Cochlear implantation via the round window membrane minimizes trauma to cochlear structures: a histologically controlled insertion study. Acta Otolaryngol. 124, 807–812.

Azaripour, A., Lagerweij, T., Scharfbillig, C., Jadczak, A.E., Willershausen, B., Van Noorden, C.J.F., 2016. A survey of clearing techniques for 3D imaging of tissues with special reference to connective tissue. Prog. Histochem. Cytochem. 51, 9–23.

Basu, S., Saha, P.K., Roszkowska, M., Magnowska, M., Baczynska, E., Das, N., Plewczynski, D., Wlodarczyk, J., 2018. Quantitative 3-D morphometric analysis of individual dendritic spines. Sci. Rep. 8, 3545.

Braun, S., Ye, Q., Radeloff, A., Kiefer, J., Gstoettner, W., Tillein, J., 2011. Protection of inner ear function after cochlear implantation: compound action potential measurements after local application of glucocorticoids in the Guinea pig cochlea. ORL (Oto-Rhino-Laryngol.) (Basel) 73, 219–228.

Buytaert, J., Goyens, J., De Greef, D., Aerts, P., Dirckx, J., 2014. Volume shrinkage of bone, brain and muscle tissue in sample preparation for micro-CT and light sheet fluorescence microscopy (LSFM). Microsc. Microanal. 20, 1208–1217.

Buytaert, J.A.N., Johnson, S.B., Dierick, M., Salih, W.H.M., Santi, P.A., 2013. MicroCT versus sTSLIM 3D imaging of the mouse cochlea. J. Histochem. Cytochem. 61, 382–395.

Chang, A., Eastwood, H., Sly, D., James, D., Richardson, R., O'Leary, S., 2009. Factors influencing the efficacy of round window dexamethasone protection of residual hearing post-cochlear implant surgery. Hear. Res. 255, 67–72.

Choong, J.K.-L., Lo, J., Chambers, S.A., Hampson, A.J., Eastwood, H.T., O'Leary, S.J., 2019. Intracochlear tPA infusion may reduce fibrosis caused by cochlear implantation surgery. Acta Otolaryngol. 139, 396–402.

Connolly, T.M., Eastwood, H., Kel, G., Lisnichuk, H., Richardson, R., O'Leary, S., 2011. Pre-operative intravenous dexamethasone prevents auditory threshold shift in a Guinea pig model of cochlear implantation. Audiology and Audiol. Neurotol. 16, 137–144.

Dobosz, M., Ntziachristos, V., Scheuer, W., Strobel, S., 2014. Multispectral fluorescence ultramicroscopy: three-dimensional visualization and automatic quantification of tumor morphology, drug penetration, and antiangiogenic treatment response. Neoplasia 16 (1), 1.

Eastwood, H., Chang, A., Kel, G., Sly, D., Richardson, R., O'Leary, S.J., 2010. Round window delivery of dexamethasone ameliorates local and remote hearing loss produced by cochlear implantation into the second turn of the Guinea pig cochlea. Hear. Res. 265, 25–29.

Eshraghi, A.A., He, J., Mou, C.H., Polak, M., Zine, A., Bonny, C., Balkany, T.J., Van De Water, T.R., 2006. D-JNKI-1 treatment prevents the progression of hearing loss in a model of cochlear implantation trauma. Otol. Neurotol. 27 (4), 504–511.

Farhadi, M., Jalessi, M., Salehian, P., Ghavi, F.F., Emamjomeh, H., Mirzadeh, H., Imani, M., Jolly, C., 2013. Dexamethasone eluting cochlear implant: histological study in animal model. Cochlear Implants Int. 14, 45–50.

Hama, H., Hioki, H., Namiki, K., Hoshida, T., Kurokawa, H., Ishidate, F., Kaneko, T., Akagi, T., Saito, T., Saido, T., Miyawaki, A., 2015. ScaleS: an optical clearing palette for biological imaging. Nat. Neurosci. 18, 1518.

Handzel, O., Burgess, B.J., Nadol, J., 2006. Histopathology of the peripheral vestibular system after cochlear implantation in the human. Otol. Neurotol. 27, 57–64.

Ishiyama, A., Doherty, J., Ishiyama, G., Quesnel, A.M., Lopez, I., Linthicum, F.H., 2016. Post hybrid cochlear implant hearing loss and endolymphatic hydrops. Otol. Neurotol. 37 (10), 1516.

Ito, J., Kojima, K., Kawaguchi, S.J., 2001. Survival of neural stem cells in the cochlea. Acta Otolaryngol. 121, 140–142.

Jia, H., Wang, J., François, F., Uziel, A., Puel, J.-L., Venail, F., 2013. Molecular and cellular mechanisms of loss of residual hearing after cochlear implantation. Ann. Otol. Rhinol. Laryngol. 122, 33–39.

Kel, G.E., Tan, J., Eastwood, H.T., Wongprasartsuk, S., O'Leary, S.J., 2013. Early cochlear response and ICAM-1 expression to cochlear implantation. Otol. Neurotol. 34 (9), 1595–1602.

Klingberg, A., Hasenberg, A., Ludwig-Portugall, I., Medyukhina, A., Mann, L., Brenzel, A., Engel, D.R., Figge, M.T., Kurts, C., Gunzer, M., 2017. Fully automated evaluation of total glomerular number and capillary tuft size in nephritic kidneys using lightsheet microscopy. J. Am. Soc. Nephrol. 28, 452–459.

Liberman, M.C., Kujawa, S.G., 2017. Cochlear synaptopathy in acquired sensorineural hearing loss: manifestations and mechanisms. Hear. Res. 349, 138–147.

Lo, J., Sale, P., Wijewickrema, S., Campbell, L., Eastwood, H., O'Leary S, J., 2017. Defining the hook region anatomy of the Guinea pig cochlea for modeling of inner ear surgery. Otol. Neurotol. 38 (6), e179–e187.

MacDonald, G.H., Rubel, E.W., 2008. Three-dimensional imaging of the intact mouse cochlea by fluorescent laser scanning confocal microscopy. Hear. Res. 243, 1–10.

Montgomery, S.C., Cox, B.C., 2016. Whole Mount Dissection and Immunofluorescence of the Adult Mouse Cochlea. JoVE, e53561.

O'Leary, S.J., Monksfield, P., Kel, G., Connolly, T., Souter, M.A., Chang, A., Marovic, P., O'Leary, J.S., Richardson, R., Eastwood, H., 2013. Relations between cochlear histopathology and hearing loss in experimental cochlear implantation. Hear. Res. 298, 27–35.

Power, R.M., Huisken, J., 2017. A guide to light-sheet fluorescence microscopy for multiscale imaging. Nat. Methods 14, 360–373.

Puelles, V.G., van der Wolde, J.W., Schulze, K.E., Short, K.M., Wong, M.N., Bensley, J.G., Cullen-McEwen, L.A., Caruana, G., Hokke, S.N., Li, J., Firth, S.D., Harper, I.S., Nikolic-Paterson, D.J., Bertram, J.F., 2016. Validation of a three-dimensional method for counting and sizing podocytes in whole glomeruli. J. Am. Soc. Nephrol. 27, 3093.

Quesnel, A.M., Nakajima, H.H., Rosowski, J.J., Hansen, M.R., Gantz, B.J., Nadol, J.B., 2016. Delayed loss of hearing after hearing preservation cochlear implantation:

human temporal bone pathology and implications for etiology. Hear. Res. 333, 225–234.
Richardson, R.T., Atkinson, P., 2015. Atoh1 gene therapy in the cochlea for hair cell regeneration. Expet Opin. Biol. Ther. 15, 417–430.
Richardson, R.T., Wise, A.K., Thompson, B.C., Flynn, B.O., Atkinson, P.J., Fretwell, N.J., Fallon, J.B., Wallace, G.G., Shepherd, R.K., Clark, G.M., O'Leary, S.J., 2009. Polypyrrole-coated electrodes for the delivery of charge and neurotrophins to cochlear neurons. Biomaterials 30, 2614–2624.
Ridler, T., Calvard, S., 1978. Picture thresholding using an iterative selection method. IEEE Trans. Syst. Man Cybern. 8, 630–632.
Ryugo, D.K., Kretzmer, E.A., Niparko, J.K., 2005. Restoration of auditory nerve synapses in cats by cochlear implants. Science 310, 1490.
Salt, A., Hartsock, J., Gill, R., Smyth, D., Kirk, J., Verhoeven, K., 2017. Perilymph pharmacokinetics of marker applied through a cochlear implant in Guinea pigs. PloS One 12, e0183374.
Sly, D.J., Campbell, L., Uschakov, A., Saief, S.T., Lam, M., O'Leary, S.J., 2016. Applying neurotrophins to the round window rescues auditory function and reduces inner hair cell synaptopathy after noise-induced hearing. Loss Otol Neurotol 37 (9), 1223–1230.
Smeds, H., Eastwood, H.T., Hampson, A.J., Sale, P., Campbell, L.J., Arhatari, B.D., Mansour, S., O'Leary, S.J., 2015. Endolymphatic hydrops is prevalent in the first weeks following cochlear implantation. Hear. Res. 327, 48–57.
Stathopoulos, D., Chambers, S., Enke, Y.L., Timbol, G., Risi, F., Miller, C., Cowan, R., Newbold, C., 2014. Development of a safe dexamethasone-eluting electrode array for cochlear implantation. Cochlear Implants Int. 15, 254–263.
Tsuji, J., Liberman, M.C., 1997. Intracellular labeling of auditory nerve fibers in Guinea pig: central and peripheral projections. J. Comp. Neurol. 381, 188–202.
Vivero, R.J., Joseph, D.E., Angeli, S., He, J., Chen, S., Eshraghi, A.A., Balkany, T.J., Van De Water, T.R., 2008. Dexamethasone base conserves hearing from electrode trauma-induced hearing loss. Laryngoscope 118, 2028–2035.
Wilk, M., Hessler, R., Mugridge, K., Jolly, C., Fehr, M., Lenarz, T., Scheper, V., 2016. Impedance changes and fibrous tissue growth after cochlear implantation are correlated and can Be reduced using a dexamethasone eluting electrode. PloS One 11, e0147552.
Wise, A.K., Tan, J., Wang, Y., Caruso, F., Shepherd, R.K., 2016. Improved auditory nerve survival with nanoengineered supraparticles for neurotrophin delivery into the deafened cochlea. PloS One 11, e0164867.
Wong, C.C., Curthoys, I.S., O'Leary, S.J., Jones, A.S., 2012. Heavy metal staining, a comparative assessment of gadolinium chloride and osmium tetroxide for inner ear labyrinthine contrast enhancement using X-ray microtomography. Acta Otolaryngol. 133, 22–27.